



Article

New Properties and Sets Derived from the $\sqrt{2}$ -Ball Fractal Dust

Mario A. Aguirre-López ¹, José Ulises Márquez-Urbina ^{2,3} and Filiberto Hueyotl-Zahuantitla ^{1,3,*}

¹ Faculty of Sciences in Physics and Mathematics, Autonomous University of Chiapas, Tuxtla Gutierrez 29050, Mexico; marioal1906@gmail.com

² Center for Research in Mathematics, Campus Monterrey, Monterrey 66629, Mexico; ulises@cimat.mx

³ National Council of Humanities, Sciences and Technologies, Mexico City 03940, Mexico

* Correspondence: fhueyotl@conahcyt.mx

Abstract: Due to their practicality and convenient parametrization, fractals derived from iterated function systems (IFSs) constitute powerful tools widely used to model natural and synthetic shapes. An IFS can generate sets other than fractals, extending its application field. Some of such sets arise from IFS fractals by adding minimal modifications to their defining rule. In this work, we propose two modifications to a fractal recently introduced by the authors: the so-called $\sqrt{2}$ -ball fractal dust, which consists of a set of balls diminishing in size along an iterative process and delimited by an enclosing square. The proposed modifications are (a) adding a resizer parameter to introduce an interaction between the generator and generated ball elements and (b) a new fractal embedded into the $\sqrt{2}$ -ball fractal dust, having the characteristic of filling zones not covered by the previous one. We study some numerical properties of both modified resulting sets to gain insights into their general properties. The resulting sets are geometrical forms with potential applications. Notably, the first modification generates an algorithm capable of producing geometric structures similar to those in mandalas and succulent plants; the second modification produces shapes similar to those found in nature, such as bubbles, sponges, and soil. Then, although a direct application of our findings is beyond the scope of this research, we discuss some clues of possible uses and extensions among which we can remark two connections: the first one between the parametrization we propose and the mandala patterns, and the second one between the embedded fractal and the grain size distribution of rocks, which is useful in percolation modeling.



Citation: Aguirre-López, M.A.; Márquez-Urbina, J.U.; Hueyotl-Zahuantitla, F. New Properties and Sets Derived from the $\sqrt{2}$ -Ball Fractal Dust. *Fractal Fract.* **2023**, *7*, 612. <https://doi.org/10.3390/fractalfract7080612>

Academic Editors: Xiaohao Cai, Jun Luo and Liang-Yi Huang

Received: 30 June 2023

Revised: 31 July 2023

Accepted: 6 August 2023

Published: 8 August 2023



Copyright: © 2023 by the authors. Licensee MDPI, Basel, Switzerland. This article is an open access article distributed under the terms and conditions of the Creative Commons Attribution (CC BY) license (<https://creativecommons.org/licenses/by/4.0/>).

Keywords: fractal dust; iterated function system; self similarity; ball sets; mandalas; succulent plant patterns; percolation modeling

1. Introduction

1.1. Background of Fractals and IFS

Since Mandelbrot's initial works on fractals [1], there has been a growing interest in studying these geometric objects due to their intriguing theoretical properties and numerous applications in different fields (see, e.g., [2–9]). Some algorithms allow the construction of fractals; the iterated function systems (IFSs) approach is among the most common and studied of these methodologies [2]. In its deterministic form, this idea for generating fractals was introduced by Hutchinson [10] in 1981.

In the most basic form of the IFS approach, a fractal is constructed as the union of several copies of an initial generator set, usually a line or region in the \mathbb{R}^2 plane, each copy being transformed by a family of mappings. Barnsley extended Hutchinson's ideas and formulated the Hutchinson–Barnsley theory [11] of an iterated function system to construct fractals as invariant subsets of metric spaces. Some of the most recognizable fractals are indeed examples of IFS-generated sets. Examples of IFS fractals are the Cantor set, Sierpinski gasket and carpet, and von Koch curve (see, e.g., [2]).

IFS fractals have applications in different fields and circumstances, making them worth studying and justifying the necessity for new examples and properties of such ob-

jects. For instance, new IFS fractals have been conceived to approximate complex natural shapes [12], design antennas [13,14], model complex networks [15], and visualize data [16]. On the other hand, some previously known IFS fractals have inspired new developments in art [17], the design of antennas [18], the modeling of complex networks [19], and interpolation and approximation theory [20]. Additionally, there has been extensive research on the theoretical properties of this family of fractals (e.g., [21]), their extension (e.g., [22]), and their use in other fields (e.g., [23]). The references in the previous examples only considered deterministic cases; the amount of relevant works increases dramatically if we also consider random IFS fractals [24].

In this context, a particular type of IFS fractal arises: the so-called $\sqrt{2}$ -ball fractal dust [25], which was previously introduced by the authors. Such a fractal is generated by an initial set consisting of a ball B_0 of radius ρ_0 that is centered and circumscribed to a square S_0 ; the initial set is reduced and copied in each of the corners of S_0 such that the reduced squares S_{1i} share one corner with S_0 and touch the ball B_0 at only one point. Thus, the sequence of the radius of the reduced balls in the m -th iteration is given by $r_m = \frac{\rho_0}{2^m} \left(1 - \frac{1}{\sqrt{2}}\right)^m$. Another way of generating this fractal, which is more convenient for our purposes, is given by considering that the initial generator set is the union of the initial ball B_0 , the boundary ∂S_0 , and its corner copies B_{1i} , ∂S_{1i} in the 1-st iteration. This initial set is then reduced and copied in the corners of the squares S_{1i} ; this process of reducing and copying is repeated at each iteration following the IFS approach.

Here, it is important to mention that this previous fractal was designed without any specific application, but detecting some main research areas for it. This led us to explore some modifications to the fractal that close it more to reproduce patterns in the real world. Two procedures to achieve that will be detailed. The first one is related to mandalas and succulent plants, while the second one to engineered foams and other structures related to fluid dynamics.

1.2. Related Work

There are some previous works with digital methodologies to generate patterns related to our first procedure. For mandalas, which are geometric configurations of symbols, usually arranged circularly [26], several works have been reported. In [27,28], the authors propose parametrized models of the main figures used as components in the interior of mandalas and place such figures in a hierarchical structure of concentric circles to generate mandala patterns. In [29], a framework is introduced to automatically design mandala patterns, and a color-transfer-based method to colorize them. In [30], the authors use complex polynomials to create mandala patterns. Besides, there are several works about the computer-based generation of traditional art patterns found in religions such as Hinduism and Buddhism. Examples of few references in this direction are the following: Refs. [31–34] generate Islamic geometric patterns, Refs. [35–37] Indian Kolam patterns, and Refs. [38–40] painting artworks. To the knowledge of the authors, there are no works that report the design of mandalas from a fractal construction, although there is one work relating fractals to Hindu temples and cosmology patterns [41].

Regarding succulents, which are a kind of plant with thickened parts to retain water in dry environments [42], we are not aware of literature dealing with the modeling and generation of succulent plants explicitly. However, some previous references have dealt with plant modeling and digital generation. For example, ref. [43] identifies a geometrical equation, “the Superformula”, capable of modeling various shapes, including those of plants. Following this work, the authors in ref. [44] use the Superformula for modeling in botany, focusing on flowers and floral organs. In ref. [45], the authors use deep learning to generate synthetic images of plant leaves to generate synthetic observations to train image recognition algorithms.

The second procedure generates a configuration similar to 2D foams, such as bubbles and sponges. Numerous studies have focused on diverse aspects of the structure of foams due to their importance in microfluids and other topics. That is, ref. [46] studied the dy-

dynamic forces acting on a bubble. Some related references for modeling the structure of bubbles include [47], which introduces a bubble scale model known as “the bubble model” that successfully replicates features of foam rheology, while [48] expands this work to include other aspects into the model. Ref. [49] presents a 2D model for contacting bubbles that can be extended to simulate 2D foams. Aqueous foams’ physical and physicochemical properties, together with some models for these phenomena, are discussed in [50]. In particular, it presents models for the structure of bubble monolayers (quasi-2D foams). The book [50] is also a good reference for modeling foams. Specialized foam models, such as the Kelvin foam, have shown a potential use in high-performance cushion materials [51].

The forms induced by the second proposal could also help to model percolation through some porous media and filters consisting of grain/rock elements covering a wide range of sizes. In this regard, ref. [52] presents a model based on the arrangement of elastic spherical particles for retention curves. In turn, ref. [53] implemented a Universal Distinct Element Code (UDEEC) model, which includes a Voronoi tessellation, to simulate the distribution of granite rocks and measure crack initiation under stress.

1.3. Problem Description and Objectives

Motivated by the circular pattern of the $\sqrt{2}$ -ball fractal dust ($\sqrt{2}$ -BFD), its simplicity and malleability in construction, and the shape of structures described in Section 1.2, this work aims to establish new frameworks and mathematical models to describe structures and phenomena in the real world. Specifically, our proposal consists of two main procedures derived from $\sqrt{2}$ -BFD, with their respective particular objectives:

- In the first one, we consider a sequence of sets with the same structure as the initial generator set (one large ball and four smaller balls), but with a dynamical interaction between the radii of the balls depending on the previous value of the sequence through a specific formula. In this case, the k -th iteration of this set is given by the union of the k first elements in the sequence. This construction breaks the original fractal nature but maintains the properties of an IFS. With the purpose of explaining the properties of the new IFS and delimiting the conditions for which the nature patterns arise, we categorize the resulting modifications regarding a parameter α , which denotes the interaction level (Section 2.1). Then, in Section 3, for a group of radii regimes, we study these sets’ asymptotic behavior, compute their Hausdorff dimension and the area they cover, and graphically illustrate the resulting sets. We also study the ratio between the sizes of the generator balls of each iteration.
- In the second one, we add new balls to the sets $B_0, B_{1,i}$, following a set of rules in such a way that the generated IFS approaches to the boundary of B_0 . That is, in our analysis, we avoid including and depicting balls and squares belonging to $m \geq 2$, while filling spaces between B_0 and $B_{1,i}$. The way of construction allows for conserving a fractal shape that resembles nontouching fluid dynamic structures, such as bubbles that intend adding to a main body, or well, fragments of rock suspended in a solution; it is detailed in Section 2.2. With the objective of detailing some of its properties and performing a comparative analysis with the first procedure, we make similar calculations and computations for this case, which are shown in Section 3 too.

In this way, our work contributes to the previous efforts in the literature from novel fractal and IFS constructions that intend to be able to reproduce structures that have the potential to be employed in different contexts (at least four). This contrasts with the specific usability of the reported methods for each context, while allowing our procedures to compete in simplicity, spatial multiscalability, and a wide set of properties that enhance the rise of new modifications. We discuss our main results for both procedures, deep into their applicability, and tag some lines for future research in Section 4. Finally, we summarize our findings in Section 5.

2. IFS-Based Methods to Modify the $\sqrt{2}$ -Ball Fractal Dust

2.1. Addition of a Resizer Parameter

Let an initial generator ball be with the radius ρ_0 and its four associated balls with the radius $\frac{\rho_0}{2} \left(1 - \frac{1}{\sqrt{2}}\right)$, which are defined by the 1-st iteration of the $\sqrt{2}$ -ball dust in a two-dimensional construction. We propose a modification of that 1-st iteration by applying an iterative interaction, tagged with the subindex k , between the generator (ρ_k) and its associated corner balls (r_k), observing that ρ_k and r_k are two sequences of radii. It is given by redefining the radii associated with the generator balls as

$$r_k = \frac{1}{2} \left(\rho_0 - \frac{\rho_{k-1}}{\sqrt{2}} \right), \quad \forall k = 1, 2, 3, \dots \tag{1}$$

$$\rho_k = \rho_0 - \alpha r_k, \quad \forall k = 1, 2, 3, \dots \tag{2}$$

where α controls the ratio between the radii sizes in each iteration. The proposed modification is equivalent to expressing Sequences (1) and (2) as

$$r_k = \rho_0 (\sqrt{2} - 1) \sum_{j=1}^k \frac{\alpha^{j-1}}{(\sqrt{2}^3)^j}, \quad \forall k = 1, 2, 3, \dots \tag{3}$$

$$\rho_k = \rho_0 - \alpha \rho_0 (\sqrt{2} - 1) \sum_{j=1}^k \frac{\alpha^{j-1}}{(\sqrt{2}^3)^j}, \quad \forall k = 1, 2, 3, \dots \tag{4}$$

so that we have two infinite sequences, $\rho = \{\rho_0, \rho_1, \rho_2, \dots\}$ and $r = \{r_1, r_2, \dots\}$, taking part in the original generator ρ_0 in its corresponding sequence. For the values of α we are interested in, the series in Equations (3) and (4) correspond to a geometric series and, therefore, can be explicitly computed. We employ this fact in our analysis below.

Then, some particular shapes or relationships between the generator and associated balls occur when $k \rightarrow \infty$ and α takes certain values. That is, we will focus on two cases that resize the balls but maintain the nontouching property ($\alpha < 2$), the inflexion case in which associated balls are touching while the generator disappears ($\alpha = 2$), and two more cases in which all the balls overlap each other by increasing their original size ($\alpha > 2$).

- Case $\alpha = 1$. The particularity of this case is the exchange ratio itself, decreasing the radius of the next generator ball (ρ_k) with the radius of the current associated balls (r_k); see Equation (2), which leads from Sequences (3) and (4) to the limits

$$\lim_{k \rightarrow \infty} r_k = \rho_0 \left(\frac{1}{3 + \sqrt{2}} \right) \tag{5}$$

$$\lim_{k \rightarrow \infty} \rho_k = \rho_0 \left(\frac{2 + \sqrt{2}}{3 + \sqrt{2}} \right). \tag{6}$$

The convergence of Equations (5) and (6) is visualized in Figure 1, in which the slight increase and decrease of r_k and ρ_k are shown, respectively. This leads to the fact that the radius ratio $\frac{\rho_k}{r_k}$ stabilizes before r_k is greater than ρ_k ; indeed, the balls corresponding to the radius r_i do not touch those ones ρ_j , $\forall i = 1, 2, \dots, j = 1, 2, \dots$, as illustrated in Figure 2 up to the 50-th iteration.

- Case $\alpha = 2$. In contrast with case $\alpha = 1$, the radius ρ_k decreases with the diameter $2r_{k-1}$. Then,

$$\lim_{k \rightarrow \infty} \sum_{j=1}^k \frac{2^{j-1}}{(\sqrt{2}^3)^j} = \frac{\sqrt{2} + 1}{2},$$

which leads to a stabilization of the radius ratio at $\frac{\rho_k}{r_k} = 0$, since

$$\lim_{k \rightarrow \infty} r_k = \frac{\rho_0}{2} \tag{7}$$

$$\lim_{k \rightarrow \infty} \rho_k = 0; \tag{8}$$

i.e., the generator ball disappears, whereas the four associated balls grow up to being tangent to each other and to the enveloping square; see Figures 1 and 3.

- Case $\alpha = \frac{1}{2-\sqrt{2}}$. This is an intermediate case to the above ones, with $1 < \alpha < 2$, which produces

$$\lim_{k \rightarrow \infty} \sum_{j=1}^k \frac{\left(\frac{1}{2-\sqrt{2}}\right)^{j-1}}{\left(\sqrt{2}^3\right)^j} = \frac{2 - \sqrt{2}}{(\sqrt{2} - 1)(3 - \sqrt{2})},$$

leading in turn to

$$\lim_{k \rightarrow \infty} r_k = \lim_{k \rightarrow \infty} \rho_k = \rho_0 \frac{2 - \sqrt{2}}{3 - \sqrt{2}}; \tag{9}$$

i.e., this case stabilizes, leading to five nontouching identical balls in size, as shown in Figure 1 and illustrated in Figure 4.

- Case $\alpha = 2^3 - (\sqrt{2})^5$. As expected by the trend shown in previous cases, ρ_k stabilizes at a negative value for cases with $\alpha > 2$. Specifically, in the present one, it produces

$$r_k = \rho_0 (\sqrt{2} - 1) \sum_{j=1}^k \frac{\alpha^{j-1}}{\left(\sqrt{2}^3\right)^j}, \quad \forall k = 1, 2, 3, \dots \tag{10}$$

$$\rho_k = \rho_0 - \alpha \rho_0 (\sqrt{2} - 1) \sum_{j=1}^k \frac{\alpha^{j-1}}{\left(\sqrt{2}^3\right)^j}, \quad \forall k = 1, 2, 3, \dots$$

and when $k \rightarrow \infty$, we obtain

$$\lim_{k \rightarrow \infty} \alpha \sum_{j=1}^k \frac{\alpha^{j-1}}{\left(\sqrt{2}^3\right)^j} = 2(\sqrt{2} + 1),$$

which leads to a stabilization at $\frac{\rho_k}{r_k} < 0$, since

$$\lim_{k \rightarrow \infty} r_k = \frac{2\rho_0}{\alpha} \tag{11}$$

$$\lim_{k \rightarrow \infty} \rho_k = -\rho_0; \tag{12}$$

i.e., the generator ball passes from diminishing its size up to recovering it as a nonphysically possible solution but mathematically, whereas the four associated balls overlap each other and are tangent in two points to the enveloping square. Figure 5 plots the iterative process considering absolute values for ρ_k . Note that, for convenience in procedure, limits (11) and (12) were obtained in a partial reverse way by looking for the value of α , observing from Equation (10) that

$$\lim_{k \rightarrow \infty} r_k = \frac{\rho_0}{(\sqrt{2}^3 - \alpha)(\sqrt{2} + 1)} \tag{13}$$

and then assuming that Equation (12) is satisfied so that

$$\alpha = \frac{8 + 2^{5/2}}{3 + 2^{3/2}} = 2^3 - (\sqrt{2})^5$$

- Case $\alpha = 1 + \sqrt{2}$. This case is similar to the latter one and produces

$$r_k = \rho_0 (\sqrt{2} - 1) \sum_{j=1}^k \frac{\alpha^{j-1}}{(\sqrt{2^3})^j}, \quad \forall k = 1, 2, 3, \dots$$

$$\rho_k = \rho_0 - \alpha \rho_0 (\sqrt{2} - 1) \sum_{j=1}^k \frac{\alpha^{j-1}}{(\sqrt{2^3})^j}, \quad \forall k = 1, 2, 3, \dots$$

and when $k \rightarrow \infty$, we obtain

$$\lim_{k \rightarrow \infty} \sum_{j=1}^k \frac{\alpha^{j-1}}{(\sqrt{2^3})^j} = 1 + \sqrt{2},$$

which also leads to a stabilization at $\frac{\rho_k}{r_k} < 0$, since

$$\lim_{k \rightarrow \infty} r_k = \rho_0 \tag{14}$$

$$\lim_{k \rightarrow \infty} \rho_k = \rho_0 (1 - \alpha); \tag{15}$$

i.e., the generator ball passes from diminishing its original size to increasing and overpassing it (in negative value), whereas the four associated balls fully overlap each other, being tangent in four points to the enveloping square; i.e., they become the original generator (see Figure 6). Similar to the latter case, limits (14) and (15) can be obtained by looking for the value of α ; namely, one can see that

$$\alpha = \frac{3 + 2^{3/2}}{2^{1/2} + 1} = 1 + \sqrt{2}$$

by using Equation (13) while assuming that (15) is fulfilled.

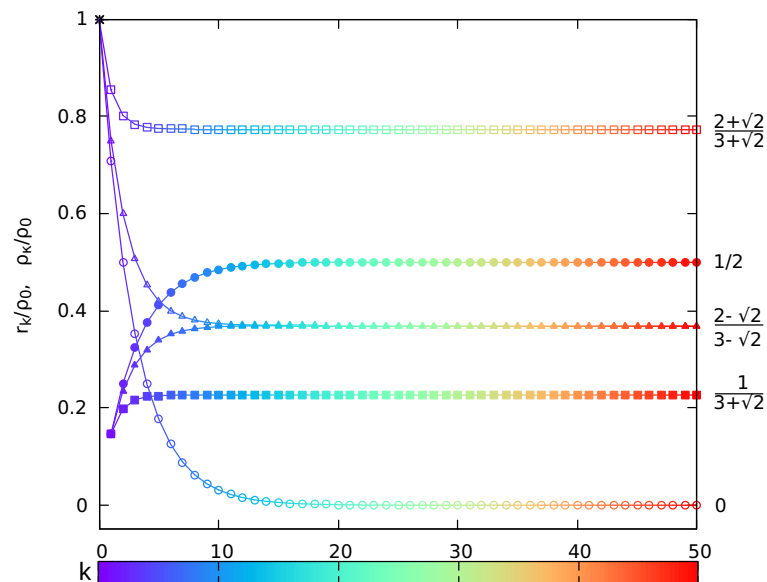


Figure 1. Evolution of the radii r_k and ρ_k (normalized to ρ_0) as a function of the number of iterations k . Cases $\alpha = 1$, $1/(2 - \sqrt{2})$, and 2 depicted as square, triangle, and circle symbols, respectively. Values of r_k are displayed with solid symbols and with open ones for ρ_k . The color scale refers to the iteration number. The corresponding values for $\lim k \rightarrow \infty$ are shown on the right axis. Although the radii seem to have converged for $k < 30$, extra values are included to agree in color scale with the convergence shown in the figures below.

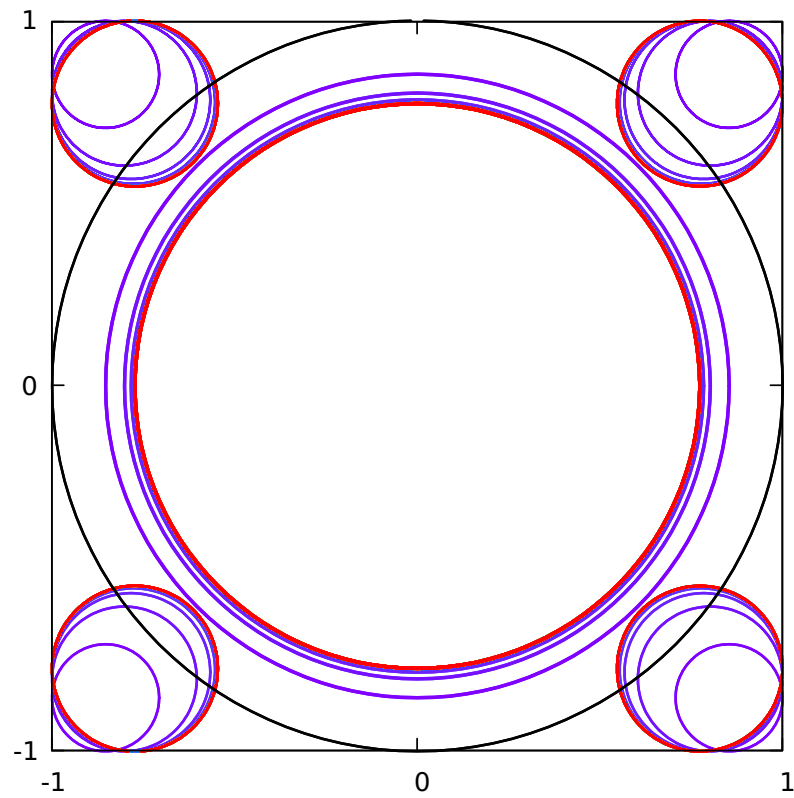


Figure 2. Case $\alpha = 1$, up to the 50-th iteration. Circles are colored according to the iteration number, following the color scale shown in Figure 1. $B(\kappa_0, \rho_0)$, $\kappa_0 = (0, 0)$, $\rho_0 = 1$ units is plotted in black as a reference.

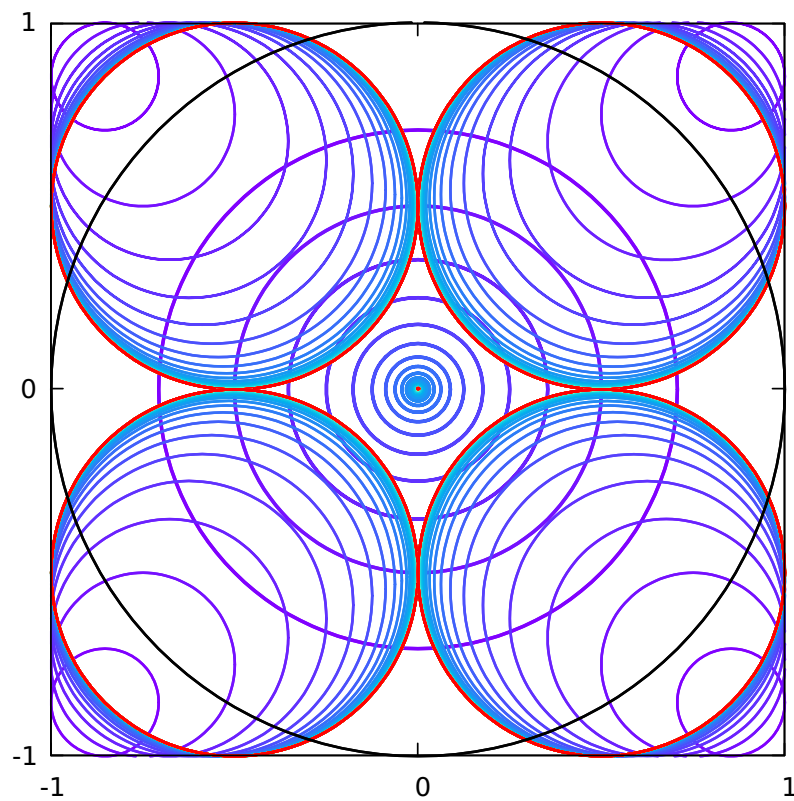


Figure 3. Case $\alpha = 2$ up to the 50-th iteration. Same notations as in Figure 2.

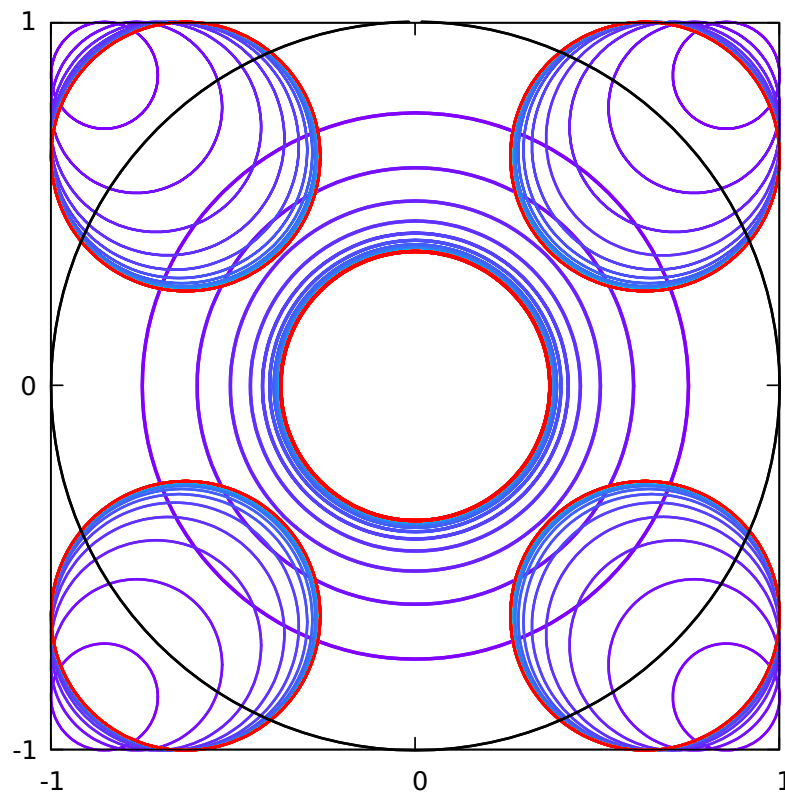


Figure 4. Case $\alpha = \frac{1}{2(1-\sqrt{2})}$ up to the 50-th iteration. Same notations as in Figure 2.

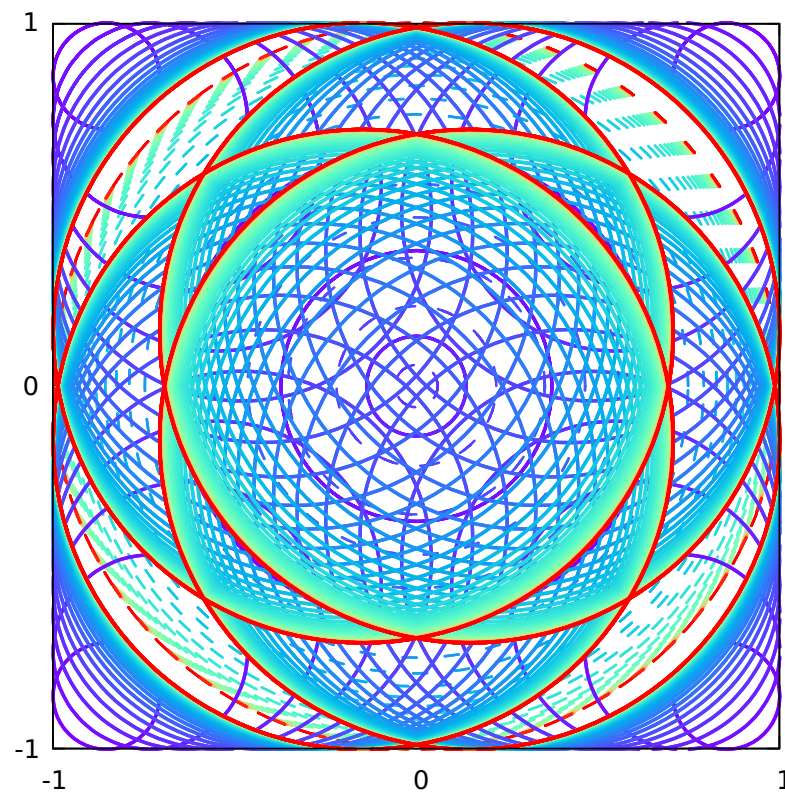


Figure 5. Case $\alpha = 2^3 - (\sqrt{2})^5$ up to the 50-th iteration. Dashed lines refer to balls with a negative radius. Same notations as in Figure 2.

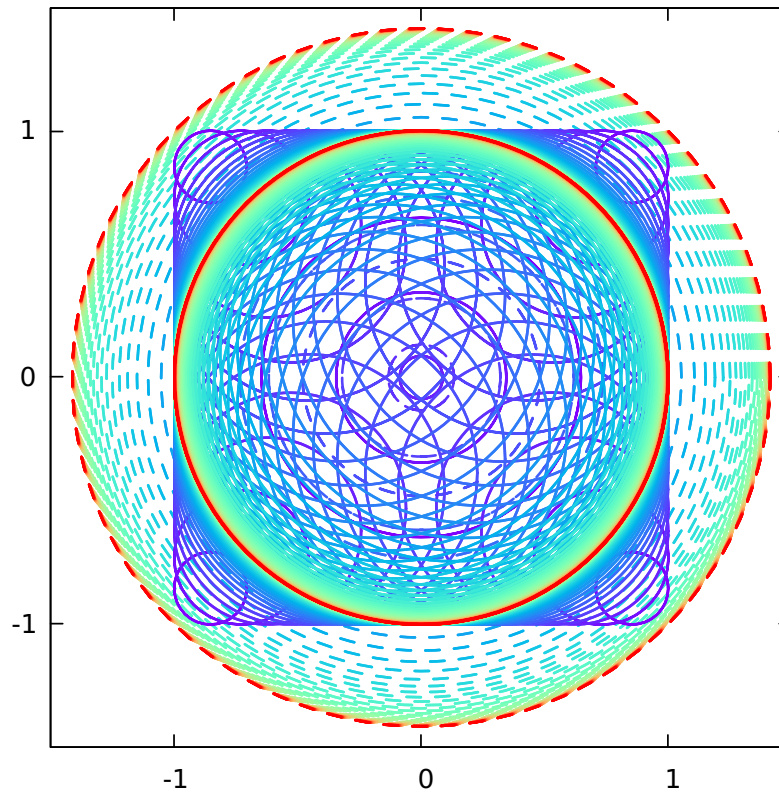


Figure 6. Case $\alpha = 1 + \sqrt{2}$ up to the 50-th iteration. Same notations as in Figure 5.

2.2. An Embedded Fractal

Let an initial generator ball be with the radius ρ_0 and its four associated balls defined by the 1-st iteration of the $\sqrt{2}$ -BFD, as for the α 's cases in Section 2.1. Starting from those balls, we propose an additional step for that 1-st iteration by adding a new embedded fractal G that follows a similar IFS construction. That is, the 0-th iteration of the new fractal is defined by $G_0 = \bigcup_{i=1}^4 \mathcal{B}(\kappa_i, \rho_i)$, with $\mathcal{B}(\kappa_i, \rho_i)$, being computed by the balls $B(\kappa_i, \rho_1)$, $i = 1, 2, 3, 4$ that are located at the corners of the enveloper square; the ball belonging to the 0-th iteration, and located at the top-right corner, is shown in Figure 7.

Then, at the 1-st iteration, $\mathcal{B}(\kappa_1, \rho_1)$ generates the two largest squares $(\mathcal{S}(\kappa_5, \rho_5), \mathcal{S}(\kappa_6, \rho_6))$ inside $S(\kappa_0, \rho_0)$ that fulfill the following:

- Touch the boundary $\partial B(\kappa_0, \rho_0)$ at only one different point $\{x_5, x_6\} \in \mathbb{R}^2, x_6 \neq x_5$.
- Do not touch any previous ball but only the boundary of their generator $\partial \mathcal{B}(\kappa_1, \rho_1)$,
- They are only path-connected by their square generator $\mathcal{S}(\kappa_1, \rho_1)$ so that the intersecting points agree with $\|x_6 - x_1\| < \|x_6 - x_5\|$.

Thus, the couples of parameters defining the two generated squares are obtained by the fulfillment of the following constraints:

$$\kappa_i \in S(\kappa_0, \rho_0), \quad \kappa_i \notin B(\kappa_0, \rho_0), \quad \bigcap_i \kappa_i = \emptyset, \quad i = 5, 6 \tag{16}$$

$$\rho_5 = \frac{1}{2} \sup \left\{ \delta_5 : \left(\mathcal{S}(\kappa_5, \delta_5) \subset S(\kappa_0, \rho_0), \mathcal{S}(\kappa_5, \delta_5) \cap \bigcup_{i=1}^4 \mathcal{S}^\circ(\kappa_i, \rho_i) = \emptyset, \right. \right. \tag{17}$$

$$\left. \left. \partial \mathcal{S}(\kappa_5, \delta_5) \cap \partial \mathcal{S}(\kappa_1, \rho_1) \neq \emptyset, \mathcal{S}(\kappa_5, \delta_5) \cap B(\kappa_0, \rho_0) = x_5 \right) \right\}, \quad \forall \delta_5 > 0.$$

$$\rho_6 = \frac{1}{2} \sup \left\{ \delta_6 : \left(S(\kappa_6, \delta_6) \subset S(\kappa_0, \rho_0), S(\kappa_6, \delta_6) \cap \bigcup_{i=1}^5 S^\circ(\kappa_i, \rho_i) = \emptyset, \right. \right. \tag{18}$$

$$\left. \left. \partial S(\kappa_6, \delta_6) \cap \partial S(\kappa_1, \rho_1) \neq \emptyset, S(\kappa_6, \delta_6) \cap B(\kappa_0, \rho_0) = x_6, \|x_6 - x_1\| < \|x_6 - x_5\| \right) \right\}, \quad \forall \delta_6 > 0.$$

Equations (16)–(18) can be applied to determine the rest of the 1-st iteration balls, this by substituting the corresponding subindexes to obtain the balls numbered by $j = 7, \dots, 12$ from their corresponding generators $j = 2, 3, 4$. Thus, the balls $B(\kappa_j, \delta_j), j = 5, \dots, 12$ make up G_1 . See Figure 7 to visualize the balls corresponding to the top-right corner, belonging from the 1-st to the 10-th iteration; as shown in the picture, each couple of generated balls corresponds to one located on the left, while another at the bottom of their generator ball (this applies to the top-right corner; however, the directions are reversed depending on the selected corner).

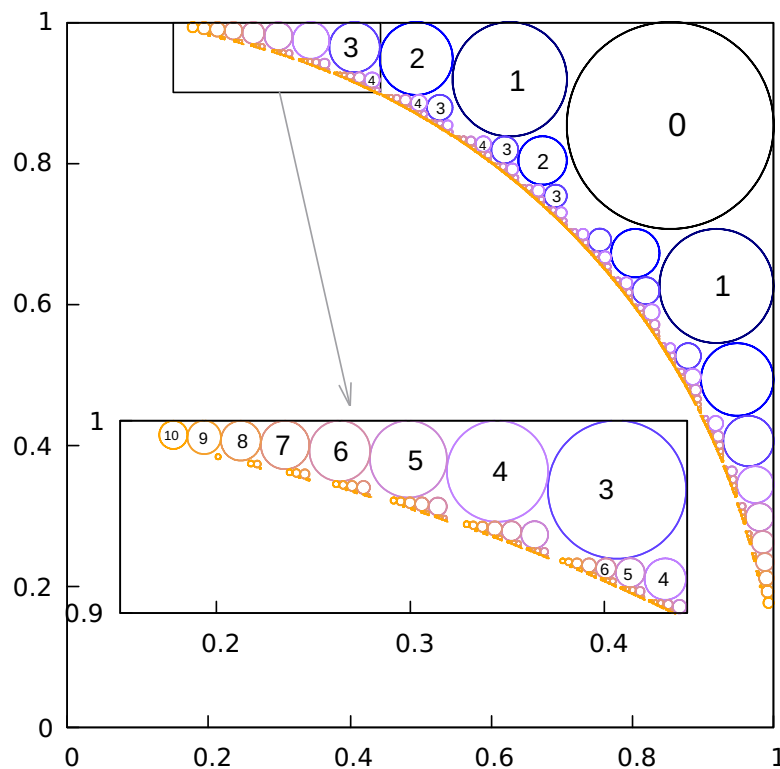


Figure 7. Top-right corner of the $\sqrt{2}$ -ball-boundary dust up to the 10-th iteration, considering an initial generator $B(\kappa_0, \rho_0), \kappa_0 = (0, 0), \rho_0 = 1$ units. Numbers and colors of the balls refer to the iteration at which the corresponding ball belongs to.

The process is then extended to the μ -th iteration, taking the balls belonging to G_1 as generators and applying Equations (16)–(18) to them. Since we start from four balls (one at each corner), and each ball generates two balls more, the number of balls generated at the μ -th iteration is given by $N_\mu = 4(2^\mu)$. In this way, the fractal is defined properly as follows:

Definition 1. Let $G_{\mu,q}$ be the q -th ball generated at the μ -th iteration of the IFS described above; then

$$G_\mu = \bigcup_{q=1}^{N_\mu} G_{\mu,q}$$

and this new ball-gasket fractal consists of

$$G = \lim_{\mu \rightarrow \infty} G_{\mu}, \tag{19}$$

which we will refer to as the $\sqrt{2}$ -ball-boundary dust, $\sqrt{2}$ -BBD.

The name of the gasket comes from the fact that when k increases, smaller balls approximate $\partial B(\kappa_0, \rho_0)$.

3. Results

Table 1 illustrates some properties of the sets constructed in Section 2. That is, the table contains the percentage area A of the initial square S_0 that such sets cover and their respective Hausdorff dimension \dim_H . Table 1 also contains the percentage area A of the initial square S_0 that the generator balls in the first and final (limit as $k, \mu \rightarrow \infty$) iterations (stages) cover in each of the cases considered. For $\sqrt{2}$ -BBD, to compare with the other sets, we consider the union of G and the ball B_0 that it delimits (see Figure 7); more precisely, we modify the generator set in the first iteration for G by redefining it as the union of the sets of the original initial iteration and B_0 . Thus, the sets in the initial stage represent about 85.3% of S_0 in all cases. Notice that the area contained by the constructed sets, which result from the union of the sets in all iterations (stages) as in any IFSs, is above 90%. Besides, the Hausdorff dimension of such sets is 2; this computation follows straightforwardly from the monotonic property of such a dimension.

For the construction with the resizer parameter, Table 1 shows that the area of the constructed sets (union) increases nonlinearly as a function of α . The increments soar abruptly after $\alpha = 2$, which is directly related to changes in the size of the radii ρ_k and r_k , as suggested by the parametric study displayed in Figure 8a. In this figure, the limits are plotted in red, and it can be observed that such limits are reached slower as the value of α increases. Figure 8b illustrates the approximated linear behavior followed by the ratio ρ_k/r_k as a function of α . Table 1 also reveals that the filled area by the generator balls in the final iteration is generally smaller than the area covered by the generator balls in the initial iteration, except for case $\alpha = 1 + \sqrt{2}$. An explanation for this monotonicity is that the overlapping areas between the ball with the radius ρ_k and the four balls with the radii r_k increase as a function of k ; however, this is not directly observable in Figure 8. Similarly, it can also be observed that the covered area by the initial stage does not follow a monotone pattern with respect to the final stage as a function of α . This phenomenon occurs despite the decreasing behavior of ρ_k/r_k .

Regarding fractal G , Table 1 indicates that the area of its generator sets in its modified initial iteration is 85.3%, which passes to 0% at the final stage (composed of a dust of miniballs with the radius $\rho_{\mu} \rightarrow 0, \mu \rightarrow \infty$). Additionally, the area of the union of the sets in all iterations fills about 95.4%. Notice that after the second iteration, the elements in this union consist entirely of points in $S_0 \cap B_0^c$, covering almost all the space out of B_0 .

Table 1. General modifications on properties of the fractal $\sqrt{2}$ -BBD, caused by the IFSs described in Section 2. Percentage area is relative to the enclosing initial square S_0 . It is measured (or calculated) at the initial, final (limit), and union stages of the respective IFSs. For cases with $\alpha > 2$, areas are filled considering balls with the absolute value of their radii.

Property	Stage	$\alpha = 1$	$\alpha = \frac{1}{2-\sqrt{2}}$	$\alpha = 2$	$\alpha = 2^3 - (\sqrt{2})^5$	$\alpha = 1 + \sqrt{2}$	$G + B_0$
A (%)	Initial	85.3	85.3	85.3	85.3	85.3	85.3
	Final	63.1	53.6	78.5	84.4	157.1	0.0
	Union	91.6	96.1	97.9	99.6	157.1	95.4
\dim_H	-	2	2	2	2	2	2

For the $\sqrt{2}$ -ball-boundary dust (G), Figure 9 depicts the number of new balls in each iteration μ and their respective radii in the logarithmic scale. There, we can observe that the largest ball in each iteration is several orders of magnitude larger than the smaller balls; this difference increases as a function of the iteration parameter μ . The size of the largest balls stabilizes as the number of iterations increases, and the size of the largest and smallest balls can be described approximately by a line as a function of μ . It is also worth noting that the balls' sizes exhibit a clustered behavior. Looking into the detail, the number of different ball sizes for $\sqrt{2}$ -BBD increases with the number of iterations, such that there are $2^{\mu-1}$ ball sizes presented at the μ -th iteration, $\forall \mu = 1, 2, 3, \dots$. Thus, observe that each size is present in eight balls (two per corner) per iteration, connected to the number of balls per iteration N_μ , as introduced in Section 2.2.

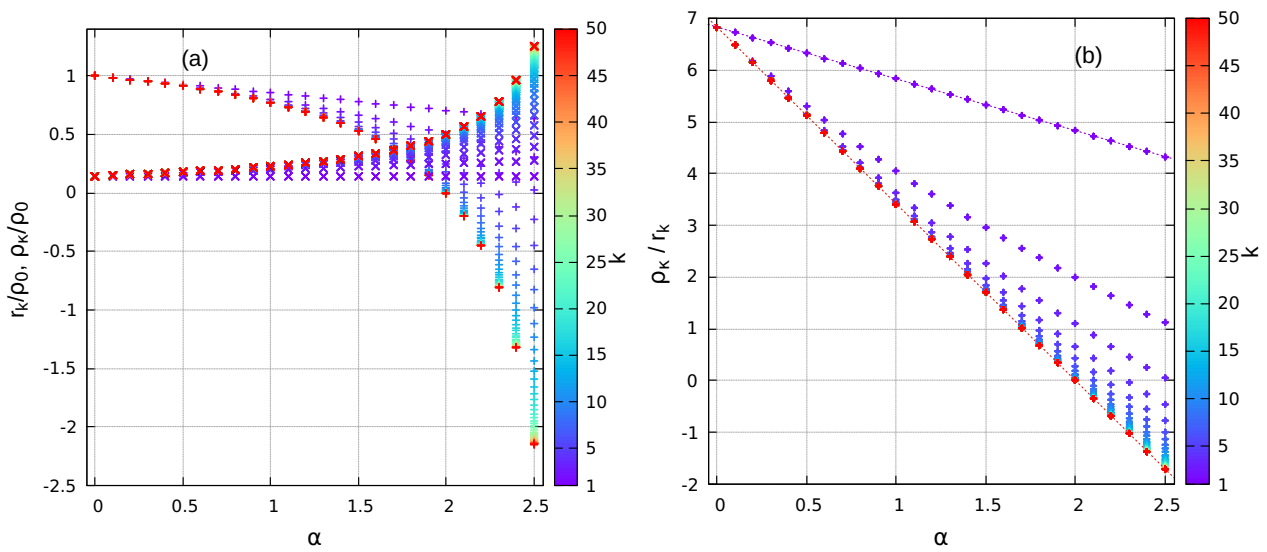


Figure 8. (a) Change in relative radius size of the generated balls, ρ (plus sign) and r (x-sign), regarding the value of α and the iteration number starting from $k = 1$ (in color scale as shown in Figure 1). (b) Ratio between the sequences of the radii (ρ, r) as a function of α .

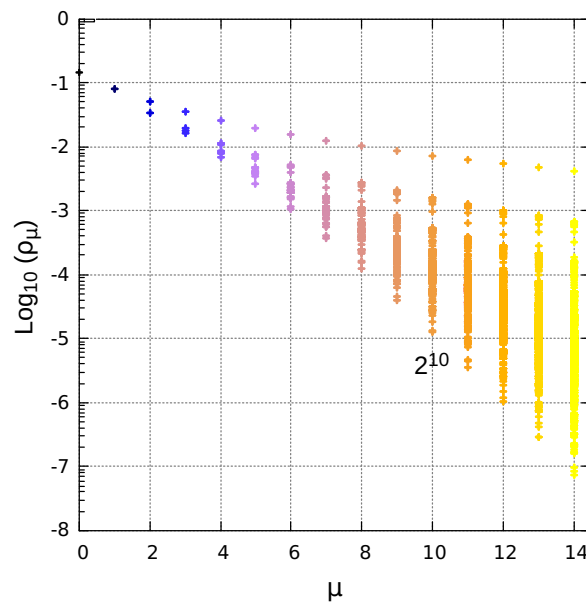


Figure 9. The figure shows the log-scaled radii of the balls added in each iteration μ in constructing the $\sqrt{2}$ -ball-boundary dust. The color scale goes according to the iteration, as in Figure 7. The number of balls generated at the 10-th iteration is indicated.

4. Discussion

4.1. First Procedure: Plants and Mandalas' Patterns

In the previous sections, we presented several figures to graphically portray some behaviors and properties of the proposed modifications of $\sqrt{2}$ -BFD. For the first modification, Figures 2–6 show different patterns depicted by the boundary of the generating balls as a function of the resizer parameter α . These figures, generated by the α -parametrization, exhibit structures similar to those encountered in mandalas and succulent plants. Thus, the proposed modifications of the fractal could be used to describe and generate these structures, providing a variety of shapes based on the parametric modeling of the fractal or determining new features to characterize, such as has been reported for trees (see [54–56] and the fractal canopy in [1]). Furthermore, our methodology brings a smooth transition of shapes by simply varying the parameter α . As shown in panels of Figure 10, mandalas are generated for values $\alpha > 2$, offering a wide catalogue of circular patterns that include shaping petals for $2.05 \leq \alpha \leq 2.25$, and succulent plants at least for $2.25 \leq \alpha \leq 2.35$ and then returning at $\alpha = 2.50$.

Although the above observations are brief, they lead to some implications but highlight the novelty and benefits that our first procedure provides, namely,

- The method establishes a connection between fractals/IFSs and mandalas. This could seem a trivial case since a trained eye could detect the appearance of fractal structures on them; however, no previous works regarding the construction of mandalas (and succulent plants) from IFSs have been reported, as mentioned in Section 1.2.
- In fact, most of the methods for designing mandalas are of an artistic type, taking only into account the maintenance of symmetry; see also the online generator [57] as a practical example. In this sense, our procedure introduces mathematical formality to construct those patterns while illustrating their asymptotic behavior as a form to understand their possible complexity (Table 1 and Figures 1 and 8). This involves the increasing of the knowledge about the geometrical properties that a mandala could possess, while enhancing the exploration of other fractals for those purposes.
- Finally, since mandalas are widely used as coloring therapy to reduce anxiety and other disorders about mental health, the exploration of new geometries, such as that generated by us, is important when looking for improving effectiveness (see [58,59] and the references therein). Therefore, this first procedure could be explored in future medical/psychological works to determine its feasibility.

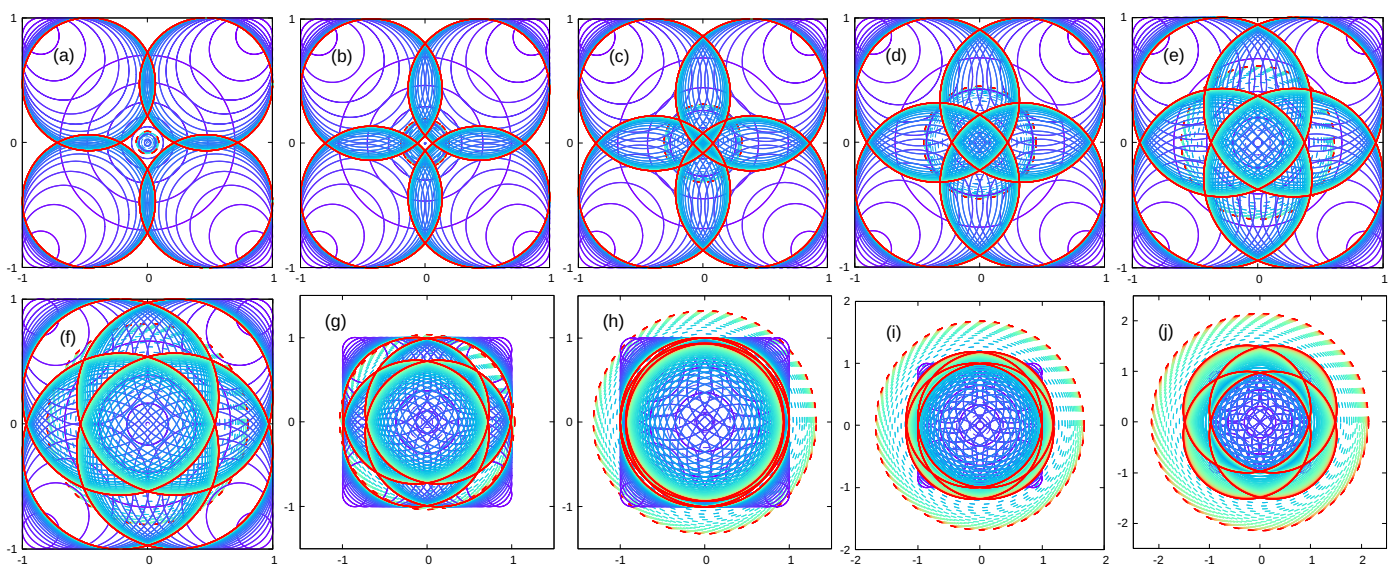


Figure 10. Ten different mandala patterns generated with procedure 1 by taking $\alpha = 2.05, 2.10, 2.15, \dots, 2.50$, which are tagged by (a–j), respectively. The color scale agrees with Figure 1.

4.2. Second Procedure: Bubble and Percolation Models

The structure depicted in Figure 7 resembles that found in soap bubbles, where smaller bubbles surround the boundary of a large bubble. This aspect suggests that $\sqrt{2}$ -BBD could provide a model to describe and understand the dynamics involved, and potentially model different types of foams, not just bubbles. In turn, Figure 7 also suggests the usage of our second procedure in percolation modeling through porous materials and filters consisting of individual grain/rock elements of different sizes. As a matter of fact, the density of $\sqrt{2}$ -BBD is a relevant parameter for applications in percolation and the modeling of bubbles and sponges since it should be directly related to the filtration level and the materials' characteristics.

The discussion of the above cues is improved by the benefits and limitations mentioned in the following items:

- The structures induced by our proposal allow for including multiple scales governed by the number of iterations in a clear way (Figure 9). This property (multiscaling) is useful for realistic simulations of the fluid dynamics' phenomena that we deal with in this work and improves the original $\sqrt{2}$ -BFD, since the multiscaling transition includes variation in circle sizes inside each iteration while decreasing them with a wide bank of sizes throughout iterations. This also contrasts with the works cited in Section 1.2, such as [52], which are feasible but do not include a multiscale approach.
- Together with the multiscaling property, we could mention the simplicity in construction as the second benefit. This involves not only the feasibility in programming but also the quickness in iterations for reproducing small structures, as also shown in Figures 7 and 9.
- The two points above make our procedure compete also in feasibility for specific problems. Indeed, as seen in Figure 11, $\sqrt{2}$ -BBD fits better (with a maximum iteration number of $\mu = 5, 7, 10$) to real data of granite size distribution than the UDEC model proposed by [53]. Although our technique is evidently limited by the structures it can construct (only nontouching circles), the procedure can be adjusted to approximate other geometric sets in cases where such an object interacts at different scales with the medium surrounding it. As a hint for that, users could add roughness to the generated structures by means of the fact that $\sqrt{2}$ -BBD intends to delineate the limit of the boundary of a circle at higher iterations.

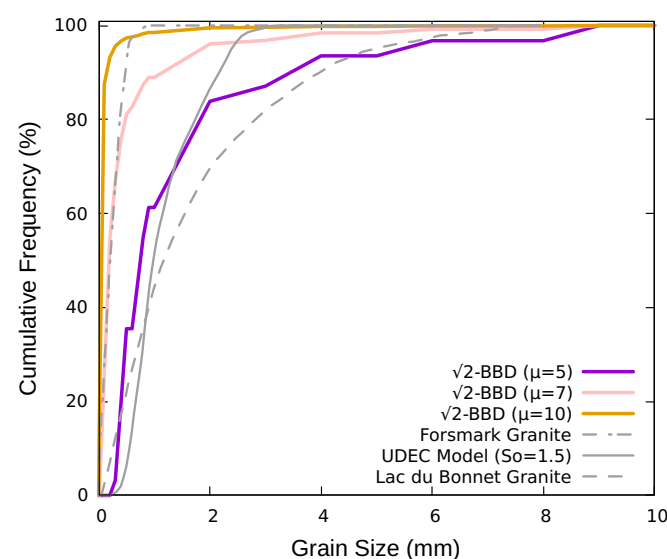


Figure 11. Comparison of reproducing grain size distribution frequency for two subtypes of granite rocks based on [60] (dashed lines). Our model is tagged by continuous colored lines, while the UDEC model ($So = 1.5$) with gray ones represents the better fitting obtained by [53]. Gray curves were approximated from Figure 8 of ref. [53].

Therefore, even though we must keep in mind that other approaches could produce more realistic forms that include irregular polygons, $\sqrt{2}$ -BBD produces a framework simple enough to test and simulate theories and models for real-world phenomena that could be an initial point to create more intricate models. Additionally, our ideas provide the foundation to obtain a richer class of sets by adding other modifications to our proposals or other fractals.

4.3. Future Research

The first research line to explore is the extension of our procedures to a 3D space, which could include the addition of a step consisting of altering the 3D construction. This change should produce new structures in the space that could include fractals even more closer to shapes in nature, which is remarkable since not all fractals have the extension property to 3D or higher dimensions while conserving feasibility in applications. Among the suggested modifications, we could mention to repeat the construction algorithm of $\sqrt{2}$ -BFD for each of the squares delineated in each iteration of $\sqrt{2}$ -BBD in order to fully cover the initial square. Additionally, for $\sqrt{2}$ -BBD fractal, a pending work is to compute its perimeter's length and Hausdorff dimension.

The next recommendations for future research consist of increasing the fitting of our procedures to the four application cases we discussed in this work, namely, modeling patterns of mandalas (1), plants (2), foams (3), and percolation structures (4). Some examples would be (a) the addition of asymmetry that expands the styles for (1) and shapes more natural silhouettes for (3) and (4); (b) customization of the IFS for (1) and (2) by adding another parameter that increase the variety of shapes; and (c) exploration of related areas by combining the developed procedures in such a way that the main iterative process could include an embedding subprocess that is started if a threshold is exceeded under certain scenarios.

5. Conclusions

Two IFSs were designed to modify the structure of the $\sqrt{2}$ -ball fractal dust. Those procedures provided new potential frameworks and mathematical models to aid in describing structures and phenomena in different contexts of the real world. Our main findings and benefits are detailed in the following bullets:

- It is possible to recursively generate a set of structures resembling mandalas and succulent plants with the first procedure (Figure 10), effectively providing an algorithm to produce geometric objects based on simple rules and equations. This last part is an advantage of our approach over others. The study included the computation of the area covered by sets generated with different values of the resizer parameter α —we do it only for some values since the general case is too intricate, and further research is required to unveil a possible formula. According to the Hausdorff dimension (HD), the resulting IFSs are not considered a fractal.
- The second procedure generates a configuration similar to that found in foams, bubbles, and sponges. Our proposal enriches the existing literature in modeling and generating such structures with a procedure based, again, on simple rules and equations. Another potential benefit of our second proposal is that it could also help model percolation through porous materials and filters consisting of grains of different sizes, which is supported by performing a direct comparison with the grain size frequency of granite rocks (Figure 11). We call the resulting set of the second modification of the $\sqrt{2}$ -ball-boundary dust. For this case, the HD also indicates that the set is not a fractal by these criteria, although the resulting structure exhibits multiscaling properties.

Author Contributions: Conceptualization, M.A.A.-L.; methodology, M.A.A.-L., J.U.M.-U. and F.H.-Z.; software, F.H.-Z.; validation, J.U.M.-U. and F.H.-Z.; formal analysis, M.A.A.-L. and J.U.M.-U.; investigation, J.U.M.-U. and F.H.-Z.; resources, J.U.M.-U.; data curation, M.A.A.-L.; writing—original draft preparation, M.A.A.-L., J.U.M.-U. and F.H.-Z.; writing—review and editing, M.A.A.-L., J.U.M.-U. and F.H.-Z.; visualization, F.H.-Z.; supervision, F.H.-Z.; project administration, M.A.A.-L. All authors have read and agreed to the published version of the manuscript.

Funding: This research received no external funding.

Institutional Review Board Statement: Not applicable.

Informed Consent Statement: Not applicable.

Data Availability Statement: No new data were created or analyzed in this study. Data sharing is not applicable to this article.

Acknowledgments: The authors thank Roberto Soto-Villalobos and Francisco Gerardo Benavides-Bravo for their feedback at the initial stage of this research.

Conflicts of Interest: The authors declare no conflict of interest.

References

1. Mandelbrot, B.B.; Mandelbrot, B.B. *The Fractal Geometry of Nature*; WH Freeman: New York, NY, USA, 1982; Volume 1.
2. Banerjee, S.; Hassan, M.K.; Mukherjee, S.; Gowrisankar, A. *Fractal Patterns in Nonlinear Dynamics and Applications*; CRC Press: Boca Raton, FL, USA, 2020.
3. Gokyildirim, A. Circuit Realization of the Fractional-Order Sprott K Chaotic System with Standard Components. *Fractal Fract.* **2023**, *7*, 470. [[CrossRef](#)]
4. Ivanov, D. Identification of Fractional Models of an Induction Motor with Errors in Variables. *Fractal Fract.* **2023**, *7*, 485. [[CrossRef](#)]
5. Joshi, M.; Agarwal, A.K.; Gupta, B. Fractal image compression and its techniques: A review. In *Soft Computing: Theories and Applications: Proceedings of SoCTA 2017*; Springer: Singapore, 2019; pp. 235–243.
6. Metzke, K.; Adam, R.; Florindo, J.B. The fractal dimension of chromatin—A potential molecular marker for carcinogenesis, tumor progression and prognosis. *Expert Rev. Mol. Diagn.* **2019**, *19*, 299–312. [[CrossRef](#)] [[PubMed](#)]
7. Leggett, S.E.; Neronha, Z.J.; Bhaskar, D.; Sim, J.Y.; Perdikari, T.M.; Wong, I.Y. Motility-limited aggregation of mammary epithelial cells into fractal-like clusters. *Proc. Natl. Acad. Sci. USA* **2019**, *116*, 17298–17306. [[CrossRef](#)]
8. Liu, S.; Bai, W.; Zeng, N.; Wang, S. A fast fractal based compression for MRI images. *IEEE Access* **2019**, *7*, 62412–62420. [[CrossRef](#)]
9. Mandelbrot, B.B. *Fractals and Scaling in Finance: Discontinuity, Concentration, Risk. Selecta Volume E*; Springer Science & Business Media: New York, NY, USA, 2013.
10. Hutchinson, J.E. Fractals and self similarity. *Indiana Univ. Math. J.* **1981**, *30*, 713–747. [[CrossRef](#)]
11. Barnsley, M.F. *Fractals Everywhere*; Academic Press: Cambridge, MA, USA, 2014.
12. Guérin, E.; Tosan, E.; Baskurt, A. Fractal coding of shapes based on a projected IFS model. In Proceedings of the 2000 International Conference on Image Processing (Cat. No. 00CH37101), Vancouver, BC, Canada, 10–13 September 2000; Volume 2, pp. 203–206.
13. Ezhumalai, A.; Ganesan, N.; Balasubramanian, S. An extensive survey on fractal structures using iterated function system in patch antennas. *Int. J. Commun. Syst.* **2021**, *34*, e4932. [[CrossRef](#)]
14. Palanisamy, S.; Thangaraju, B.; Khalaf, O.I.; Alotaibi, Y.; Alghamdi, S.; Alassery, F. A Novel Approach of Design and Analysis of a Hexagonal Fractal Antenna Array (HFAA) for Next-Generation Wireless Communication. *Energies* **2021**, *14*, 6204. [[CrossRef](#)]
15. Carletti, T.; Righi, S. Weighted fractal networks. *Phys. A Stat. Mech. Its Appl.* **2010**, *389*, 2134–2142. [[CrossRef](#)]
16. Chan, E.Y.; Corless, R.M. Chaos game representation. *SIAM Rev.* **2023**, *65*, 261–290. [[CrossRef](#)]
17. Soo, S.; Yu, K.M.; Chiu, W. Modeling and fabrication of artistic products based on IFS fractal representation. *Comput.-Aided Des.* **2006**, *38*, 755–769.
18. Guariglia, E. Harmonic Sierpinski gasket and applications. *Entropy* **2018**, *20*, 714. [[PubMed](#)]
19. Sun, W.; Zhang, J.; Wu, Y. Novel evolving small-world scale-free Koch networks. *J. Stat. Mech. Theory Exp.* **2011**, *2011*, P03021.
20. Paramanathan, P.; Uthayakumar, R. Fractal interpolation on the Koch Curve. *Comput. Math. Appl.* **2010**, *59*, 3229–3233.
21. Falconer, K.; Fraser, J.; Jin, X. Sixty years of fractal projections. In *Fractal Geometry and Stochastics V*; Springer: Cham, Switzerland, 2015; pp. 3–25.
22. Rajan, P.; Navascués, M.A.; Chand, A.K.B. Iterated functions systems composed of generalized θ -contractions. *Fractal Fract.* **2021**, *5*, 69.
23. Lin, C.H.; Wu, J.X.; Li, C.M.; Chen, P.Y.; Pai, N.S.; Kuo, Y.C. Enhancement of chest X-ray images to improve screening accuracy rate using iterated function system and multilayer fractional-order machine learning classifier. *IEEE Photonics J.* **2020**, *12*, 1–18.
24. Ghosh, R.; Marecek, J. Iterated Function Systems: A Comprehensive Survey. *arXiv* **2022**, arXiv:2211.14661.
25. Soto-Villalobos, R.; Benavides-Bravo, F.G.; Hueyotl-Zahuantitla, F.; Aguirre-López, M.A. A new deterministic gasket fractal based on ball sets. In Proceedings of the WSCG 2023: Computer Science Research Notes, Prague, Czech Republic, 15–19 May 2023; pp. 306–314. [[CrossRef](#)]

26. Wikipedia Contributors. Mandala—Wikipedia, The Free Encyclopedia, 2023. Available online: <https://en.wikipedia.org/wiki/Mandala> (accessed on 28 June 2023).
27. Zhang, J.; Zhang, K.; Peng, R.; Yu, J. Computer-aided generation of mandala thangka patterns. In Proceedings of the 10th International Symposium on Visual Information Communication and Interaction, Bangkok, Thailand, 14–16 August 2017; pp. 93–100.
28. Zhang, J.; Zhang, K.; Peng, R.; Yu, J. Parametric modeling and generation of mandala thangka patterns. *J. Comput. Lang.* **2020**, *58*, 100968.
29. Xu, S.; Zhang, Y.; Yan, S. Automatic mandala pattern design and generation based on COOM framework. *J. Comput. Lang.* **2022**, *72*, 101138.
30. Poelke, K.; Tokoutsis, Z.; Polthier, K. Complex Polynomial Mandalas and their Symmetries. In Proceedings of the Bridges 2014: Mathematics, Music, Art, Architecture, Culture, Seoul, Republic of Korea, 14–19 August 2014; pp. 433–436.
31. Karam; Nakajima. Islamic symmetric pattern generation based on group theory. In Proceedings of the 1999 Proceedings Computer Graphics International, Canmore, AB, Canada, 7–11 June 1999; pp. 112–119.
32. Lu, P.J.; Steinhardt, P.J. Decagonal and quasi-crystalline tilings in medieval Islamic architecture. *Science* **2007**, *315*, 1106–1110.
33. Cromwell, P.R. The search for quasi-periodicity in Islamic 5-fold ornament. *Math. Intell.* **2009**, *31*, 36–56.
34. Beatini, V. Kinetic rosette patterns and tessellations. *Int. J. Comput. Methods Exp. Meas.* **2017**, *5*, 631–641.
35. David, N.; Robinson, T.; Thomas, D.; Balamurugan, B.; Samuel, S. Graph grammars for kolam patterns and honeycomb patterns. *Int. J. Math. Sci.* **2007**, *6*, 355–367.
36. Pradella, M.; Cherubini, A.; Reghizzi, S.C. A unifying approach to picture grammars. *Inf. Comput.* **2011**, *209*, 1246–1267.
37. Gopalan, V.; VanLeeuwen, B.K. A Topological Approach to Creating any Pulli Kolam, an Artform from Southern India. *arXiv* **2015**, arXiv:1503.02130.
38. Sugihara, K. Computer-aided generation of Escher-like sky and water tiling patterns. *J. Math. Arts* **2009**, *3*, 195–207.
39. Lin, S.S.; Morace, C.C.; Lin, C.H.; Hsu, L.F.; Lee, T.Y. Generation of escher arts with dual perception. *IEEE Trans. Vis. Comput. Graph.* **2017**, *24*, 1103–1113.
40. Tao, W.; Liu, Y.; Zhang, K. Automatically generating abstract paintings in Malevich style. In Proceedings of the 2014 IEEE/ACIS 13th International Conference on Computer and Information Science (ICIS), Taiyuan, China, 4–6 June 2014; pp. 201–205.
41. Trivedi, K. Hindu temples: Models of a fractal universe. *Vis. Comput.* **1989**, *5*, 243–258. [[CrossRef](#)]
42. Wikipedia Contributors. Succulent Plant—Wikipedia, The Free Encyclopedia, 2023. Available online: https://en.wikipedia.org/wiki/Succulent_plant (accessed on 28 June 2023).
43. Gielis, J. A generic geometric transformation that unifies a wide range of natural and abstract shapes. *Am. J. Bot.* **2003**, *90*, 333–338.
44. Gielis, J.; Gerats, A. A botanical perspective on modeling plants and plant shapes in computer graphics. In Proceedings of the International Conference on Computing, Communications and Control Technologies, Austin, TX, USA, 14–17 August 2004.
45. Benfenati, A.; Bolzi, D.; Causin, P.; Oberti, R. A deep learning generative model approach for image synthesis of plant leaves. *PLoS ONE* **2022**, *17*, e0276972.
46. Manor, O.; Vakarelski, I.U.; Stevens, G.W.; Grieser, F.; Dagastine, R.R.; Chan, D.Y. Dynamic forces between bubbles and surfaces and hydrodynamic boundary conditions. *Langmuir* **2008**, *24*, 11533–11543. [[PubMed](#)]
47. Durian, D.J. Foam mechanics at the bubble scale. *Phys. Rev. Lett.* **1995**, *75*, 4780. [[PubMed](#)]
48. Durian, D.J. Bubble-scale model of foam mechanics: MMelting, nonlinear behavior, and avalanches. *Phys. Rev. E* **1997**, *55*, 1739.
49. Weaire, D.; Höhler, R.; Hutzler, S. Bubble-bubble interactions in a 2d foam, close to the wet limit. *Adv. Colloid Interface Sci.* **2017**, *247*, 491–495.
50. Cantat, I.; Cohen-Addad, S.; Elias, F.; Graner, F.; Höhler, R.; Pitois, O.; Rouyer, F.; Saint-Jalmes, A. *Foams: Structure and Dynamics*; OUP Oxford: Oxford, UK, 2013.
51. Ge, C.; Priyadarshini, L.; Cormier, D.; Pan, L.; Tuber, J. A preliminary study of cushion properties of a 3D printed thermoplastic polyurethane Kelvin foam. *Packag. Technol. Sci.* **2018**, *31*, 361–368. [[CrossRef](#)]
52. Monnet, J.; Boutonnier, L.; Taïbi, S.; Mahmutovic, D.; Branque, D. Theoretical modelling of retention curve for Livet-Gavet loam. *E3S Web Conf.* **2020**, *195*, 02015.
53. Nicksiar, M.; Martin, C. Factors Affecting Crack Initiation in Low Porosity Crystalline Rocks. *Rock Mech. Rock Eng.* **2014**, *47*, 1165–1181. [[CrossRef](#)]
54. Liu, X.; Ma, Q.; Wu, X.; Hu, T.; Dai, G.; Wu, J.; Tao, S.; Wang, S.; Liu, L.; Guo, Q.; et al. Nonscalability of Fractal Dimension to Quantify Canopy Structural Complexity from Individual Trees to Forest Stands. *J. Remote Sens.* **2022**, *2022*, 0001. [[CrossRef](#)]
55. Grigoriev, S.V.; Shnyrkov, O.D.; Pustovoit, P.M.; Iashina, E.G.; Pshenichnyi, K.A. Experimental evidence for logarithmic fractal structure of botanical trees. *Phys. Rev. E* **2022**, *105*, 044412. [[CrossRef](#)]
56. Hui, Z.; Cai, Z.; Xu, P.; Xia, Y.; Cheng, P. Tree Species Classification Using Optimized Features Derived from Light Detection and Ranging Point Clouds Based on Fractal Geometry and Quantitative Structure Model. *Forests* **2023**, *14*, 1265. [[CrossRef](#)]
57. Shilo, H. Mandala Maker, 2023. Available online: <http://mandala-app.com/> (accessed on 27 July 2023).
58. Curry, N.A.; Kasser, T. Can Coloring Mandalas Reduce Anxiety? *Art Ther.* **2005**, *22*, 81–85. [[CrossRef](#)]

59. Hosseini, M.; Borzabadi Farahani, Z. Evaluating the Effectiveness of Mandala Coloring on Mental Health in Iran: A Systematic Review. *J. Health Sci. Surveill. Syst.* **2022**, *10*, 144–149. [[CrossRef](#)]
60. Lim, S.S.; Martin, C.D.; Åkesson, U. In-situ stress and microcracking in granite cores with depth. *Eng. Geol.* **2012**, *147–148*, 1–13. [[CrossRef](#)]

Disclaimer/Publisher’s Note: The statements, opinions and data contained in all publications are solely those of the individual author(s) and contributor(s) and not of MDPI and/or the editor(s). MDPI and/or the editor(s) disclaim responsibility for any injury to people or property resulting from any ideas, methods, instructions or products referred to in the content.